Supplementary Materials for

Segmented Terahertz Electron Accelerator and Manipulator (STEAM)

D. Zhang, A. Fallahi , M. Hemmer, X. Wu, M. Fakhari, Y. Hua, H. Cankaya, A.-L.

Calendron, L. Zapata, H. Matlis, and F. X. Kärtner

correspondence to: dongfang.zhang@cfel.de

This file includes:

Materials and Methods

Supplementary Text

Fig. S1-S9

Other Supplementary Materials for this manuscript includes the following:

Movie S1

Supplementary Text

Experimental setup

The experimental setup is illustrated in Fig. 1a. The 55 keV electron beam is produced from a photo-triggered DC gun driven at 257 nm with the fourth harmonic of an IR laser beam (Yb:KYW, 1,030 nm, 550 fs, 4 mJ for high repetition demonstration or Yb:YLF, 1,020 nm, 1.1 ps, 40 mJ for high peak accelerations demonstration). Most of the IR beam is further split into two separate beams, each one generating a single-cycle THz pulse via the tilted pulse front method[1]. Currently 2×2 µJ THz pulses are available from the Yb:KYW laser (or 2×30 µJ from the Yb:YLF laser) with a center frequency of 0.3 THz (Fig. 1 inset). The THz energies delivered to the experiment are currently limited by losses in the THz beam transport. Also the coupling of the THz pulses into the STEAM device are not yet optimized, resulting in greatly reduced THz energies at the THz-electron interaction region of about 2×0.5 µJ when driven with the Yb:KYW laser system (or 2×6 µJ THz when driven with the Yb:YLF laser system). In this study, we merely focus on the amount of THz that interacts with the electron bunch in the STEAM device. The pair of THz pulses entering the STEAM device needs to overlap in space as well as in time with each other and with the electron pulse inside the cavity to produce an effective interaction. The optical time delays between the two THz pulses and the electron pulse are controlled by their relative path difference using motorized delay stages. Electrons interact with the THz field in the designed segmented THz waveguide structure (Fig. 1a inset) and are finally detected by a micro-channel plate (MCP) detector.

Segmented THz waveguide structure

Figure S1a,b show the schematic of the designed segmented waveguide structure with two horns for coupling the THz into the waveguide. The simulation model uses Gaussian beam propagation with 2×10 µJ THz energy, a pulse duration of 3.33 ps, a central frequency of 0.3 THz, a beam diameter of 0.9 mm and the simulation uses a finite-element based code[2]. The electron beam is phase synchronized with the electric field of the THz inside each layer, therefore, it gains energy continuously (Fig. S1c). While tuning the relative delay between electron and THz pulses, an energy modulation is achieved as shown in Fig. S1d.

Operation modes of the STEAM device

Figure S2 schematically illustrates different operation modes of the STEAM device. The first row corresponds to the electric mode, where the electric fields of the two counter-propagating excitations superpose to realize acceleration, compression and focusing. Figure S2a shows the temporal signature of the accelerating field (electric field along the electron beam path) in each layer, as well as a visualization of the interaction. Ideally, this field is spatially uniform in each layer. Nonetheless, the fringing field effects from adjacent layers perturb this field uniformity. Similar to conventional cavities, an electron bunch is injected at the beginning of the negative half-cycle of the field, sweeps through a half-cycle, and eventually leaves the layer at the end of the negative half-cycle. Consequently, a net energy gain is achieved from the THz beam.

When the electron bunch is injected at the peak of the negative half-cycle, the layer is completely traversed after a half-cycle and the electrons leave the beam at the peak of the positive half-cycle. Such an interaction is visualized in Fig. S2b. The net energy gain

3

of electrons is zero in each layer. However, due to finite length of the electron bunch, particles at the head of the bunch gain smaller momentum than the ones in the bunch tail. This effect reverses the energy chirp of the bunch and results in bunch compression after a propagating an additional distance. According to the Panofsky-Wenzel theorem, such bunch compression takes place in tandem with defocusing. Similarly, a bunch decompression scheme will lead to focusing of the electron beam. For this purpose, the same beam and device configuration can be used, but the electrons enter the layer when the field strength reaches its maximum at the positive cycle and leave at the minimum of the negative cycle. The corresponding magnetic field profile leading to focusing of the bunch is already shown in Fig. 5 of the main manuscript.

In order to deflect an electron beam, the transverse magnetic fields of the two beams need to superpose which leads to cancellation of the total electric field, i.e. magnetic mode operation. In this operation mode, when the particles are injected at the zero-crossing of the magnetic field, they sweep a half cycle with a constant magnetic field sign, as shown in Fig. S2c. Therefore, a total deflection of the beam is acquired.

In the same magnetic operation mode, if the bunch is injected at the minimum of the transverse magnetic field, it leaves the layer at the maximum as shown in Fig. S2d. Therefore, the total deflection of the bunch will be zero. In this interaction, the finite length of the bunch causes a streaking effect. More accurately, the particles at the bunch head deflect to one direction, whereas the particles at the tail of the bunch deflect to the opposite direction. As a result, the bunch length will be projected on to the transverse momentum, which enables bunch length measurements using a streaking device.

One may think of using the electric field instead of the magnetic field of the THz radiation inside the waveguide for deflection and streaking. In the regime of sub-relativistic electrons using the *E*-field for deflection is more efficient than the *B*-field. However, an additional problem emerges when the STEAM device is used for manipulation of sub-relativistic (here, 43% of the speed of light) electrons. In order to ensure that the electron beam will not interact with more than one half-cycle of the THz field, the thickness of the inserted dielectric material is designed to be around a quarter wave of the THz wavelength. Limited by the cut-off frequency ($\lambda/2$), the THz radiation cannot propagate into the dielectric part if a dominant transverse electric field exists in the mode, which is required for *E*-field deflection. Therefore, the *E*-field has to be perpendicular to the surface to guarantee an efficient coupling of the THz radiation and multi-layer interaction. Meanwhile this is the only way, one can achieve all operating modes: acceleration, streaking/deflection, focusing, and compression, are dynamically performed in a single device.

Sub-MeV electron acceleration

With increase of the acceleration field strength, better THz mode and smaller focus, the acceleration can be greatly enhanced. Theoretically a 450 keV (Fig. S3) electron beam can be achieved with 2×100 µJ THz energy. The layer thickness and length are also optimized (Fig. S3 inset) in order to keep the electron beam phase synchronized with the THz field.

Laser system

We have two pump laser systems, namely a Yb:KYW and a cryogenically cooled Yb:YLF laser system.

The dual-crystal Yb:KYW regenerative amplifier[3] is seeded at 1,030 nm with a 42.5 MHz Yb:KYW oscillator from Amplitude Systems. The nJ-level pulses of the oscillator are stretched by chirped fiber Bragg gratings, whose losses are compensated by ytterbium doped fiber amplifiers. The linear regenerative amplifier has 6 decades of gain, delivering 5 mJ energy per pulse. The contrast between the amplified pulse and the unamplified seed pulses is better than 100:1, measured with a photodiode. The pulses are then compressed by two passes through a Treacy compressor; the multi-dielectric gratings exhibit low losses, allowing a compression efficiency of ~80%. The 4 mJ, 1,030 nm centered pulses are measured to have a pulse duration of 550 fs assuming a $sech^2$ fit at FWHM.

The Yb:YLF system used in the experiments and presented in this paper is based on a chirped pulse amplification (CPA) architecture. Optical pulses are generated, temporally stretched and pre-amplified in a home built fiber-based front-end[4] that delivers optical pulses with 2.4 nm FWHM spectral bandwidth with up to 100 nJ energy and a stretched pulse duration of ~1 ns at 33 MHz repetition rate. These optical pulses are injected into a ring-cavity regenerative amplifier operating at 10 Hz repetition rate. The regenerative amplifier features a cryogenically cooled 25% doped, 1.75 mm long Yb:YLF gain medium pumped by a fiber coupled diode array operating at 960 nm wavelength and delivering up to 300 W peak power. A combination of half-wave plate, thin-film polarizer and a Rubidium Titanyle Phosphate (RTP) Pockels cell is used for

injection into and ejection from the amplifier. Upon amplification, the optical pulses show a 10 mJ output energy, moderate spectral narrowing to ~2.1 nm FWHM spectral bandwidth and a TEM00 spatial intensity profile[5] (Fig. S4). These 10 mJ pulses are then sent into a polarization switched 4-pass booster amplifier featuring two cryogenically cooled 25 mm-thick Yb:YLF rods pumped by a fiber coupled diode array operating at 940 nm wavelength and delivering up to 2 kW peak power in 3 ms duration. Pulses emerging from the 4-pass unsaturated amplifier show 85 mJ energy and no modification of the spectral or spatial intensity profile from the 10 mJ seed. The amplified pulses are directed toward a Treacy-type pulse compressor and show a measured duration of 1.1 ps upon compression.

THz Generation

Single-cycle THz pulses were generated via Optical rectification, using the tilted pulse front technique in a lithium niobate ($LiNbO_3$) crystal. The pulse front of the infrared laser is tilted by a 1,500 l/mm grating. One spherical lens with focal length 75 mm was used to image the titled-pulse-front onto the $LiNbO_3$ crystal. The THZ pulse energy is measured with a pyroelectric detector from Gentec Instruments.

The maximum THz energy we generated with the Yb:KYW laser is around 2×2 μJ with the $LiNbO_3$ crystal at room temperature and an input energy of 2×1.5 mJ. The generated THz radiation has a center frequency of 0.3 THz (Fig. S5a,b) that matches with the designed frequency of the STEAM device. With the Yb:YLF laser, at room temperature the generated THz has a center frequency of around 0.2 THz (Fig. S5c,d). This is far away from the designed parameter and leads to dramatic loss of THz coupling and inefficient THz-electron interaction. By cooling down the $LiNbO_3$ crystal down to 90

K, we are able to shift the center frequency to 0.29 THz and get around 2×30 µJ with an input energy of 2×19 mJ (Fig. S5e,f).

The UV laser for electron generation and the THz pulses generators are driven by the same laser system. Therefore, electrons and THz pulse are inherently synchronized with sub-fs precision. The jitter in the setup originates from drift in pointing and timing of the laser system, which is located a few meters away from the DC electron gun. The very small shot-to-shot jitter is below our streaking resolution limit. In terms of long term drift, the Yb:KYW laser system shows sufficient stability during the whole experiment below its streaking resolution limit (100 fs). With the high power Yb:YLF laser, it shows a few hundred fs drift over an hour. This is mainly due to the fact that this laser is still under development and there is no beam pointing stabilizer to stabilize drifts in pointing of the laser beam induced by temperature changes or vibrations in the lab.

Detection of deflection and acceleration

The deflection induced by the magnetic field of the THz pulse is observed on the MCP-detector in the horizontal plane. The energy-dependent deflection from the electromagnetic dipole is in the vertical plane (Fig. 1). In the figures shown in Fig. 2**e** of the main manuscript and Fig. S6, the images are rotated by 90° in order to fit with the space of the whole figure. Figure S6a shows the initial 55 keV electron beam and its projection in the horizontal (b) and vertical (c) direction that provides the energy and deflection information, respectively. In the electric mode, while the electron beam is in acceleration condition, it gives the maximum energy change. Figure S6d shows such an example of acceleration. Since the B-field is cancelled, the deflection change is also

minimized (Fig. S6f). While in the magnetic mode, maximum deflection can be seen with the energy change minimized (Fig. S6g,i).

THz deflection with the Yb:YLF laser

Limited by the designed opening angle of the STEAM device, while running at the magnetic mode with the *E*-field cancelled at the interaction point, the electrons are cut by the wall of the device at the exit with the maximum coupled THz (~2×6 µJ from the Yb:YLF laser). This can be seen from the clear cutting edge of the deflection diagram (Fig. S7a). This also gives the maximal deflection angle (~70 mrad) of the device. On the right side, in Fig. S7b, the streaking range is ~30 times larger than the unstreaked beam, which is still limited by the opening angle of the device. The square marked part of Fig. S7a shows that a peak streaking gradient of ~140 µrad/fs can be achieved with this device.

Electron bunch compression for shorter electron bunches

In the current experimental setup, the second STEAM device (streaker) is placed around 200 mm away from the first STEAM device (buncher). The simulation displayed in Fig. S8 shows that with a higher field and moving the streaker closer, even shorter electron bunches are expected. In practice the distance between streaker and buncher is limited by the initial design of the experimental configuration.

Electron bunch focusing for smaller electron bunches

In the current experimental setup, the MCP detector is placed around 180 mm away from the first STEAM device (compressor). The simulation displayed in Fig. S9 shows that with a higher field, smaller electron bunches are expected. In practice the distance

between streaker and MCP detector is limited by the initial design of the experimental
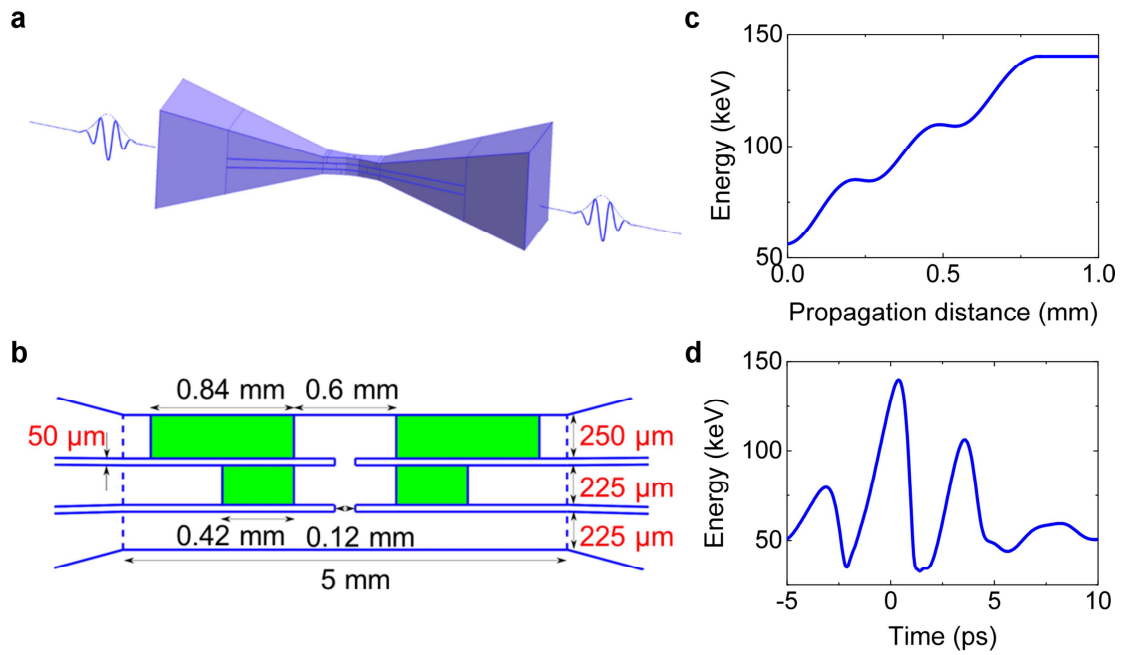
configuration.

Figure S1.a,b, Schematic illustration of the designed segmented waveguide structure. **c,** Calculated acceleration along the electron propagation direction. **d,** Simulated energy as a function of the THz-electron interaction time. Simulation is performed based on 2×10 uJ THz energy, central frequency of 0.3 THz and beam diameter of 0.9 mm.
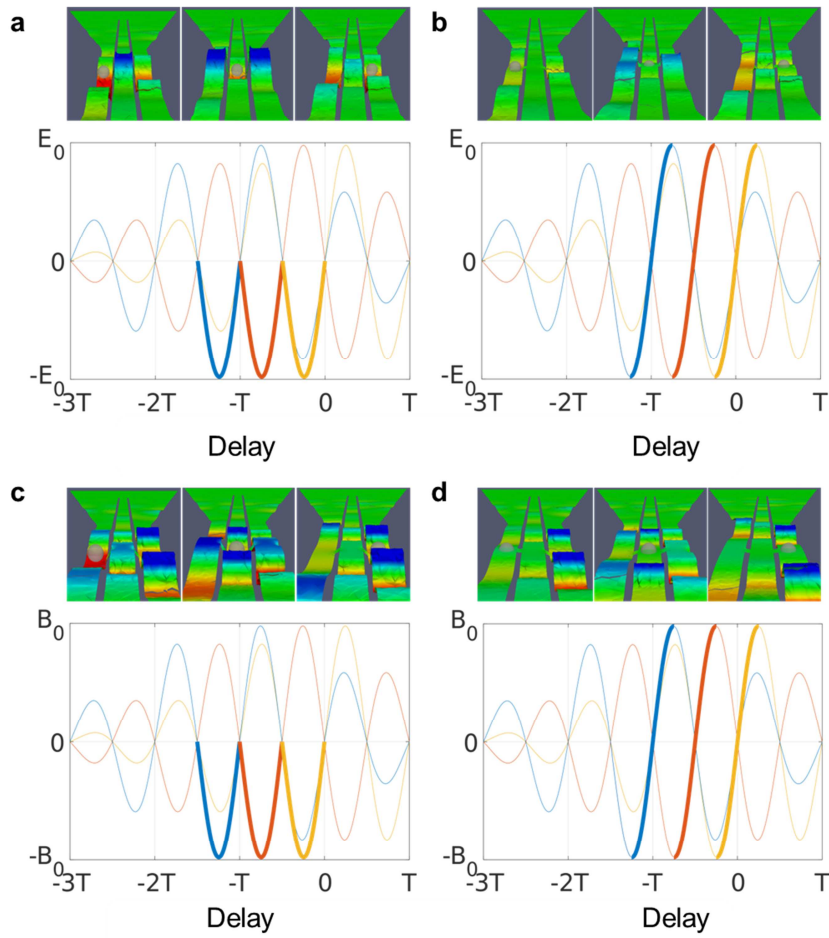
Figure S2. Different operation modes of the STEAM device: temporal signature of the electric and/or magnetic fields affecting the electron bunch as well as snapshots of the interaction are shown for (**a**) acceleration, (**b**) compression, (**c**) deflection, and (**d**) streaking regimes.
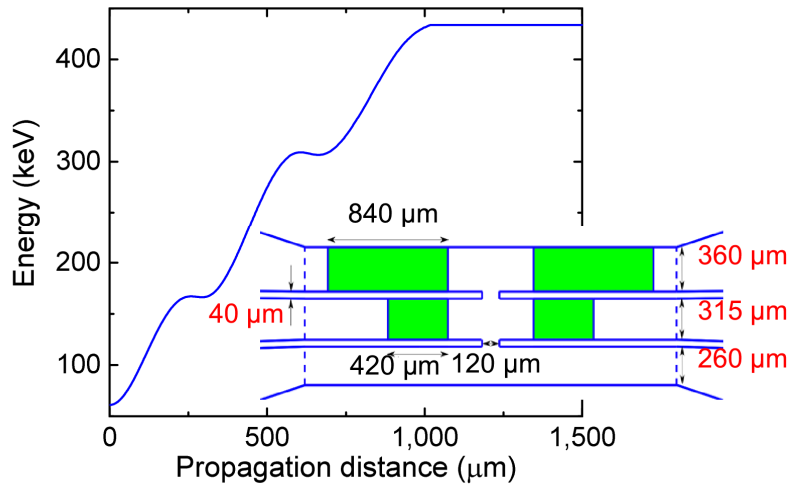
Figure S3. Acceleration of electrons with higher THz energy (2×100 uJ THz energy, central frequency of 0.3 THz and beam diameter of 0.9 mm).
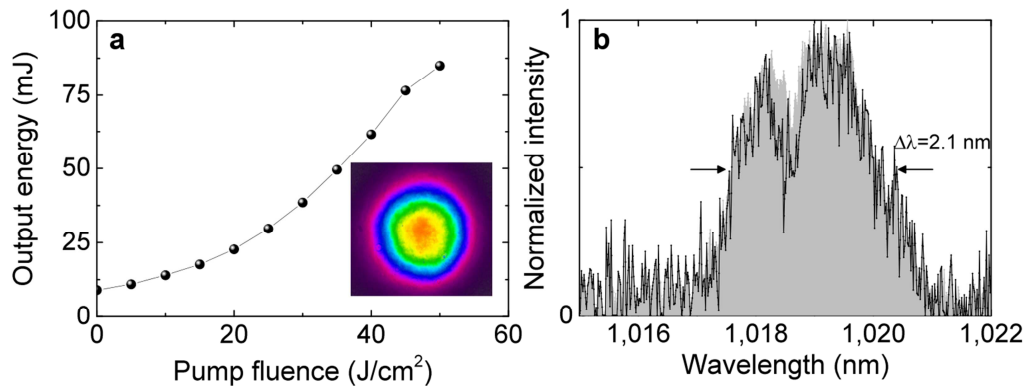
Figure S4. Measurements of the Yb:YLF laser. **a,** Measured characteristic of output energy vs pump fluence at the output of the final booster amplifier for 10 mJ seed energy and (inset) near field spatial profile measured at the output of the amplifier. **b,** Typical measured spectra at the output of the front-end seeder (grey shaded area) and at the output of the booster amplifier (black line).
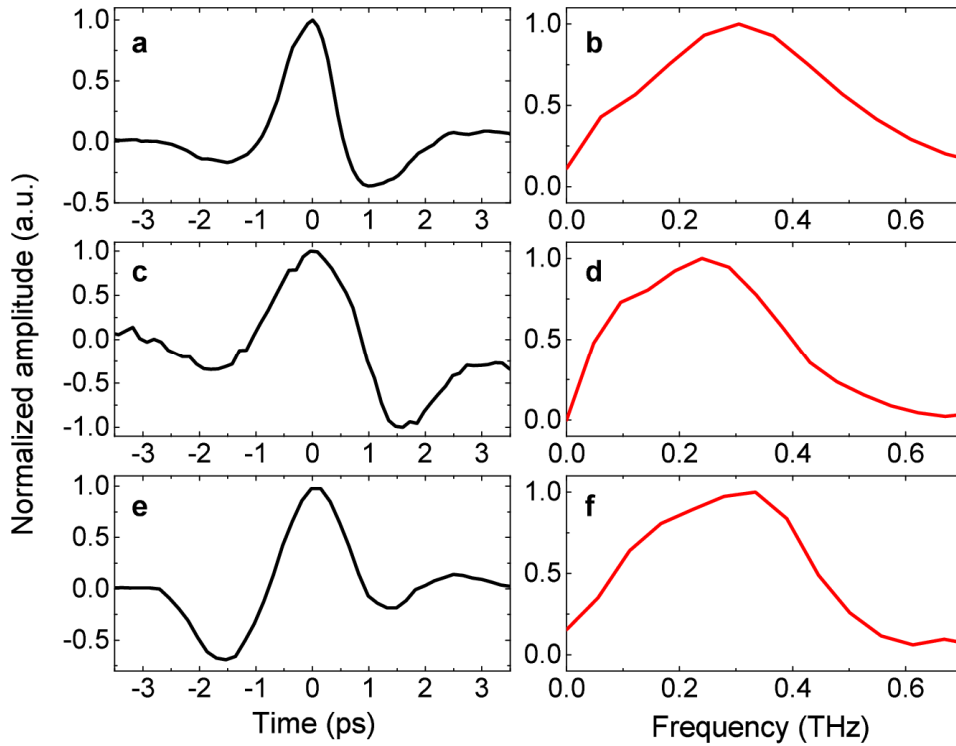
Figure S5. a and **b** Electro-optic sampling of the THz pulse generated from the Yb:KYW
laser pulse measured in the time-domain and calculated back in the frequency domain. **c**
and **d** Electro-optic sampling of the THz pulse generated from the Yb:YLF laser pulse at
room temperature (300 K) measured in the time-domain and calculated back in the
frequency domain. **e** and **f** Electro-optic sampling of the THz pulse generated from the
Yb:YLF laser at low temperature (90 K) measured in the time-domain and calculated
back in the frequency domain. The frequency domains are shown truncated to the low
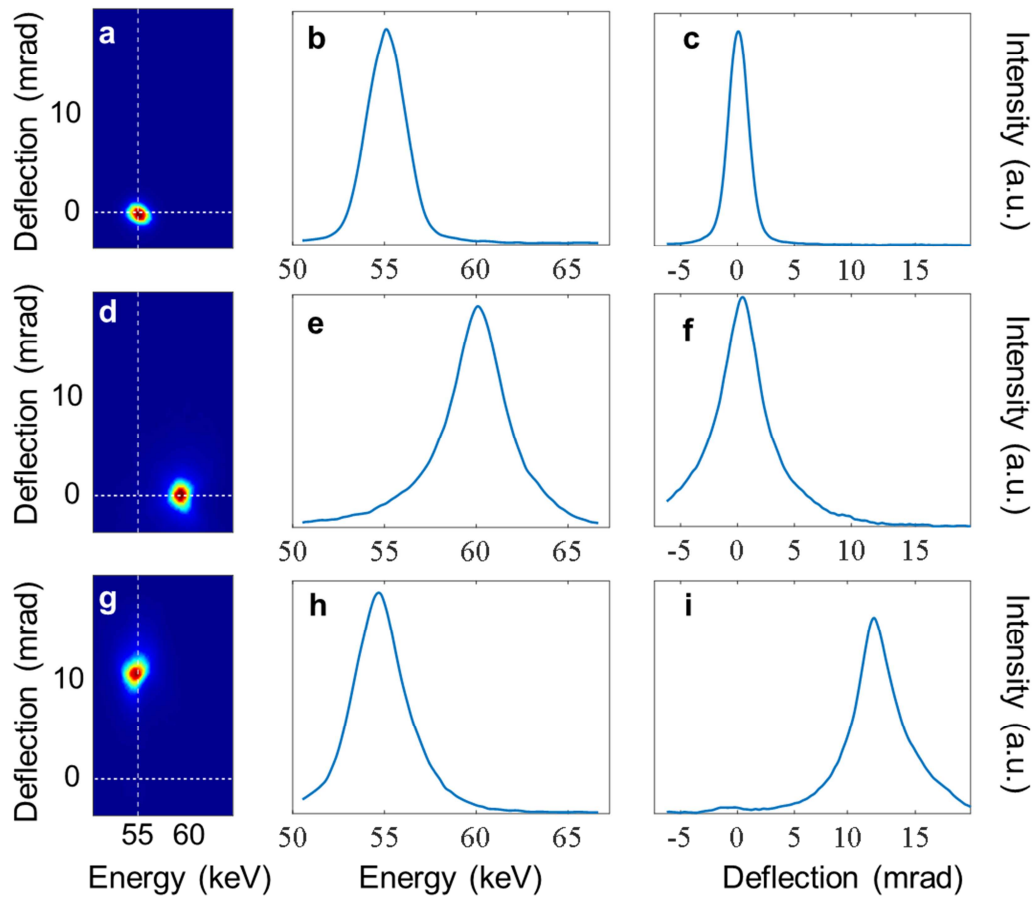energy part of the spectrum, here of interest for the experiment.

Figure S6. a, Initial 55 keV electron beam observed by the MCP-detector and its projection on the horizontal (**b**) and vertical (**c**) direction, which represent the energy and deflection change respectively. **d,** Maximal accelerated electron beam and its projection on the horizontal (**e**) and vertical (**f**) direction. **g,** Maximal accelerated electron beam and its projection on the horizontal (**h**) and vertical (**i**) direction. This demonstration was performed using the Yb:KYW laser system with ~2×0.5 μJ THz coupled into the structure and a bunch charge of ~1 fC.
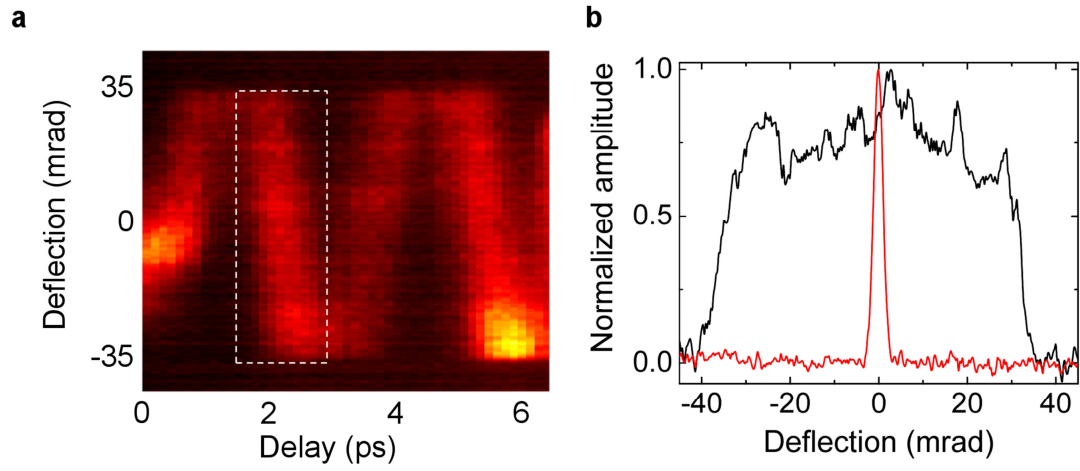
Figure S7. a, Time-dependent deflectogram measured by varying the delay between the electron pulse and the THz with the E-field cancelled. **b,** Black line: Half-cycle of the deflectogram square part in (**a**) are integrated horizontally. Red line: Unstreaked electron beam. This demonstration was performed using the Yb:YLF laser with ~2×6 µJ THz coupled into the structure and a bunch charge of ~10 fC charge.
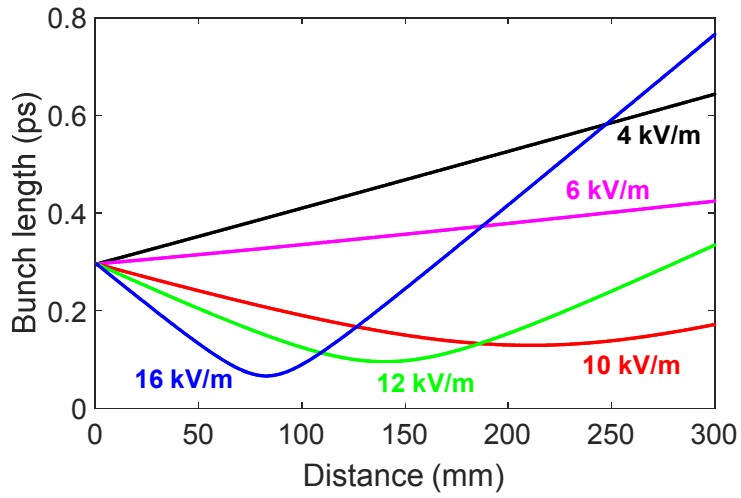
Figure S8. Simulated bunch length vs position with different THz field strength.
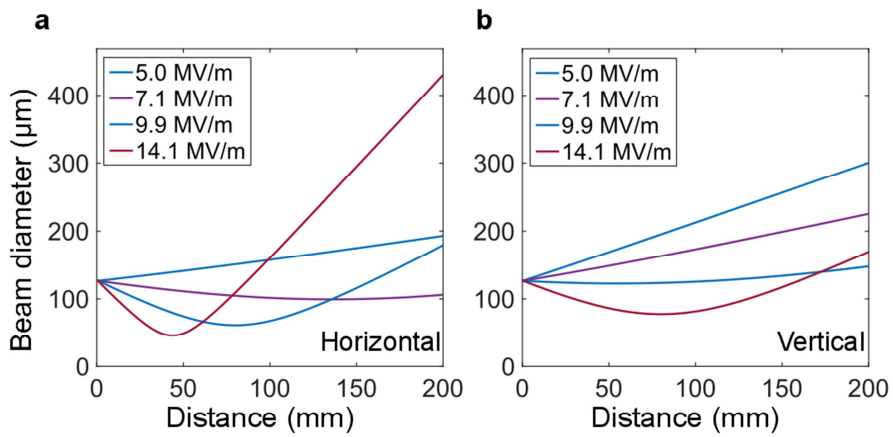

Figure S9. Simulated beam diameter vs position with different THz field strength.

Movie S1

THz field development as a function of time inside the STEAM device.

References

1. Hebling, J., Almasi, G., Kozma, I. Z. & Kuhl, J. Velocity matching by pulse front tilting for large area THz-pulse generation. *Opt. Express* **10,** 1161-1166 (2002).

2. Calendron, A.-L., Çankaya, H. & Kärtner, F. X. High-energy kHz Yb:KYW dual-crystal regenerative amplifier. *Opt. Express* **22**, 24752-24762 (2014).

3. Fallahi, A. & Kärtner, F. X. Field-based DGTD/PIC technique for general and stable simulation of interaction between light and electron bunches. *J. Phys. B* **47,** 234015 (2014).

4. Hua, Y. *et al.* 87-W, 1018-nm Yb-fiber ultrafast seeding source for cryogenic Yb:YLF amplifier. in *Conference on Lasers and Electro-Optics,* paper SM4Q.5. (2016).

5. Hemmer, M., Zapata, L., Hua, Y. & Kärtner, F. X. Addressing Spectral Narrowing in Cryogenic Yb:YAG: a 10 mJ Cryogenic Yb:YLF Regenerative Amplifier, in *Lasers Congress 2016 (ASSL, LSC, LAC),* paper ATh4A.3. (2016).